INFLUENCE OF DENSITY AND MICROSTRUCTURE ON FATIGUE PROPERTIES OF WARM COMPACTED Fe-Ni-Cu-Mo STEELS

Sven Bengtsson

Research and Development
Höganäs AB, Sweden

ABSTRACT

A common cause of failure in service is by fatigue fracture, especially of heavily loaded components subjected to dynamic stresses. The Fe-Ni-Cu-Mo steels have very high static mechanical properties and are becoming increasingly popular in highly stressed applications.

This presentation deals with the fatigue behavior of warm-compacted Fe-Ni-Cu-Mo steels. The fatigue behavior has been investigated with respect to density and microstructure. The fatigue strength was determined for several density levels in the as sintered condition and in one case for a rapidly cooled material. Fracture surfaces have been characterized with respect to the origin of the fatigue crack and size of defect at the starting point.

INTRODUCTION

Sintered components for highly loaded structural applications are becoming more and more frequent in e.g. automobiles. One of the major reasons behind this advance is that in addition to the traditional P/M advantages; cost and dimensional tolerances, also the strength and fatigue properties have improved. The use of higher densities (>7,0 g/cm^3) through improvements in compaction technology (e.g. Warm compaction) and improvements in powder quality, has boosted the properties to levels that previously were unattainable. However, pressed and sintered steels are characterized by the presence of pores. It is natural to assume that the crack initiation starts at one of these pores or at a conglomerate of pores. However, for higher densities (>7,2 g/cm^3) the largest pores available are not big enough to start stable crack growth according to present theories [e.g. 1]. This means that the crack must grow by some other mechanism to a size that allows stable crack growth to occur. By

introducing stronger microstructural components it is possible to increase the fatigue limit for an identical pore structure.

The present investigation highlights some of the differences between the diffusion alloyed D.AE and D.HP1 and the properties that can be achieved.

EXPERIMENTAL

Two diffusion alloyed powders, D.AE and D.HP1 were used in this study. The powders were mixed with graphite and lubricant using the Densmix ™, bonding technique. Table 1 shows the compositions.

The base powder for the D.AE is the pure water atomized iron powder. The alloying elements, Ni, Cu and Mo (in powder form) are mixed with the iron powder and subjected to a co-annealing process were the additives are allowed to adhere to the iron particles by diffusion. The process is allowed to continue to such a point that the additive particles stick to the iron particles. The diffusion is very limited into the iron matrix resulting in similar hardness as plain iron powder and consequently it has a high compressibility.

D.HP1 is manufactured in a similar way, but instead of plain iron powder a pre-alloyed powder with 1,5 wt.% Mo is used as a base. Nickel and copper are used as additives in powder form.

The first powder (D.AE) sinters to a mixed structure of pearlite grains in a matrix of martensite, (retained) austenite and some bainite. The pearlite is strongly influenced by the cooling rate after sintering or other post sinter heat treatments. The microstructure of the D.HP1 based material (D.HP1) consists of bainite grains in a matrix of martensite and (retained) austenite. The main difference between the two materials is the fact that the latter is based on pre-alloyed atomized powder. This means that the hardenability is higher, while the compressibility is somewhat lower.

Table 1.

Nominal composition of powder mixes.

Base powder / Code	**Composition (wt.%)**				
	Ni	**Cu**	**Mo**	**Graphite**	**Lubricant**
D.AE.	4,0	1,5	0,5	0,8	0,65
D.HP1	4,0	2,0	1,5	0,7	0,50

The test bars were pressed in a Tonitechnik 100 ton, semi-automatic laboratory press, see Table 2. The warm compaction was performed with both tool and the powder pre-heated to 130 ^{o}C (266 ^{o}F). The sintering was performed in laboratory scale belt furnaces using strict atmosphere control. The cooling rate after sintering is approximately 0,8 ^{o}C/sec (1,5 ^{o}F/sec) in the temperature range 900 - 600 ^{o}C. (1658 - 1118 ^{o}F) The rapid cooling after sintering was performed in a furnace capable of approximately 5 ^{o}C/sec (9 ^{o}F/sec) for the present component and furnace loading. After pressing and sintering the test bars were not treated in any way prior to the testing. The burr, however small, that is created between the die and the punch was allowed to remain on the test bars. A drawing of the specimens is shown in Figure 1.

Table 2.

Processing conditions for the tested materials.

Specimens were sintered at 1120 °C (2048 °F) for 30 min in a mixture of 90% N_2 / 10% H_2.

Code	Cooling rate*	Compaction pressure ** (MPa / ksi)	Sintered density (g/cm^3)
D.AE normal cooling D.AE Rapid cooling	normal high**	800 / 116	7,28
D.HP1 7,06	normal	510 / 74	7,06
D.HP1 7,25	normal	700 / 102	7,25
D.HP1 7,35	normal	820 / 119	7,35

* "Normal" cooling rate is approximately 0,8 oC/sec (1,5 oF/sec) in the temperature range 900-600 oC (1658 - 1118 oF). "High" cooling rate is approximately 5 oC/sec (9 oF/sec) in the temperature range 900-600 oC (1658 - 1118oF).

** Warm compacted with powder and tool temperature at 130 °C (266 °F)

The tensile tests were performed in a MTS Sintech 20D tensile tester by evaluating 7 samples per material. The gauge length was 25 mm and the specimens were pulled at 1 mm/min up to 1% total strain and then with 2 mm/min.

The fatigue tests were performed as axial push - pull tests with a stress ratio of -1, i.e. the stress is alternating between a positive and negative (compressive) axial stress of the same magnitude. The tests were carried out in a Roell Amsler HP5100 high frequency pulsator at 160 Hz. The fatigue limit for 50% survival was set to $2 \cdot 10^6$cycles. The test were performed and evaluated using the stair case method. In most cases at least 20 and in some cases up to 25 test bars were used. The stair case method is a convenient way to determine the fatigue strength for 50% survival at $2 \cdot 10^6$ cycles with a good accuracy using a relatively low number of specimens. The first test was started at a pre-selected load (best guess). If the specimen breaks the load is lowered one increment, in this case 10 MPa (1,5 ksi). If the specimen survives $2 \cdot 10^6$cycles without failure, it is considered a run out. The next test load will be increased one increment. This procedure continues until 15-25 specimens are tested. The test loads used will exhibit a concentration around the 50% survival load and, without using elaborate statistical evidence, this fact can be said to be the reason behind the good accuracy of the determination of the 50% fatigue strength. It is also possible to determine a value of the scatter, usually in the form of the standard deviation, the 90% fatigue strength or any similar measure. However, caution must be exercised when interpreting the scatter since this is an entity that is very sensitive to single deviating tests. In this paper, the term 'fatigue strength' will be used instead of the more precise, but long expression: the fatigue strength for 50% survival at $2 \cdot 10^6$ cycles.

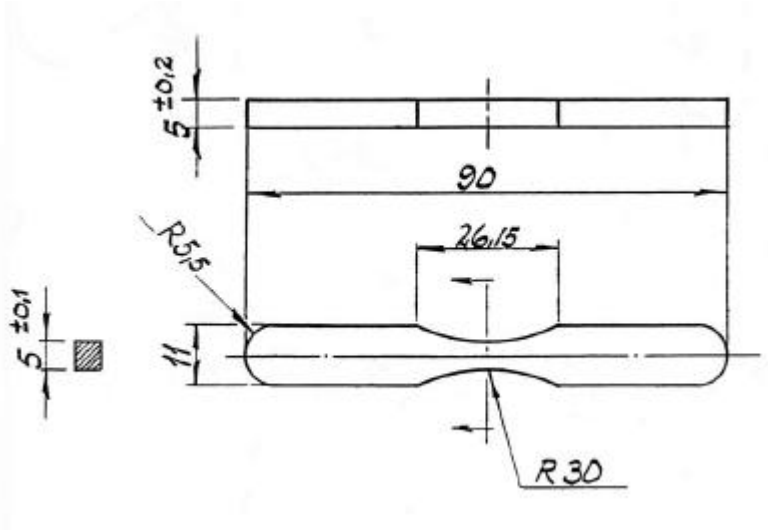


Figure 1. Drawing of fatigue test bar.

Image analysis was performed on fatigue tested samples. The samples were mounted in resin, ground and polished using standard metallographical techniques. The image analysis was carried out using a Leica microscope and a Quantimet 500 IW image analyzer. At least 32 image fields of approximately 1000 by 800 micron were used for each analysis. The image was recorded, grey scale thresholds set and its features were measured. The measurements were compiled into a histogram of number of pores in each pore size class. The maximum length of the pore was used as the measure of the pore size. The pore frequency was defined as the number of pores in each class divided by the measured area.

RESULTS

Material D.AE exhibits a longer purely elastic part of the stress - strain curve for the rapidly cooled material compared to the conventionally cooled material, see Figure 2a. It also exhibirts a faster deformation hardening rate. This behavior result in higher yield strength for the rapidly cooled material compared to the material with normal cooling rate. However, the overall ductility and the ultimate tensile strength are somewhat lower. The tensile tests of D.HP1 are shown in Figure 2b.

Table 3.

Selected mechanical properties of the tested materials.

Material	Fatigue strength (MPa / ksi)	Rm (MPa / ksi)	R_{p02} (MPa / ksi)	Elongation (%)	Density (g/cm^3)
D.AE based material					
Normal cooling 0.8 °C/sec / 1.5 °F/sec					
D.AE	185 / 27	700 / 102	450 / 65	2,1	7,11
D.AE	217 / 31	790 / 115	450 / 65	1,5	7,26
D.AE	240 / 35	n/a	n/a	n/a	7,40
Rapid cooling 5 °C/sec / 9 °F/sec					
D.AE	285 / 41	710 / 103	550 / 80	0,5	7,26
D.HP based material					
As sintered condition					
D.HP1	215 / 31	830 / 120	460 / 67	1,0	7,06
D.HP1	253 / 37	860 / 125	570 / 83	0,9	7,25
D.HP1	305 / 44	930 / 135	590 / 86	1,0	7,35

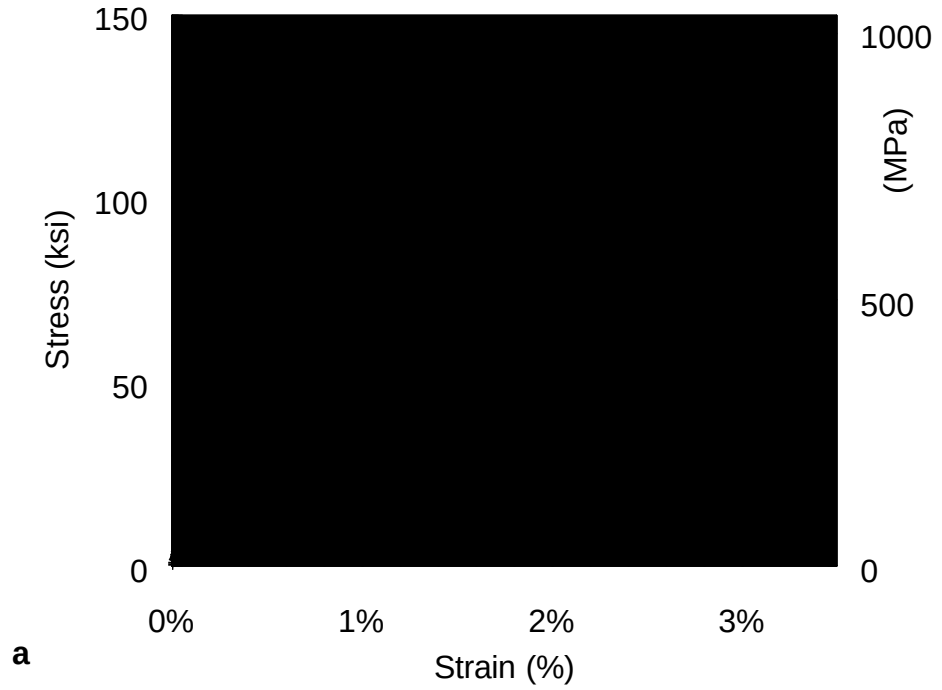


Figure 2a. Stress - strain diagram from tensile tests of material D.AE in the normally cooled and rapidly cooled versions.

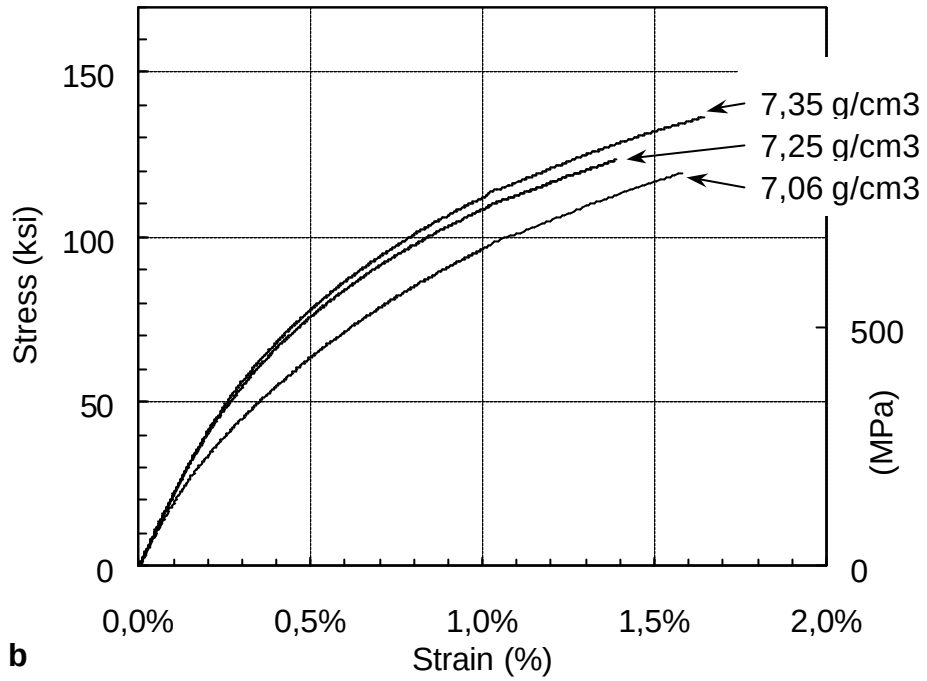


Figure 2b. Stress - strain diagram from tensile tests of material D.HP1 at densities 7,06, 7,25 and 7,35 g/cm^3.

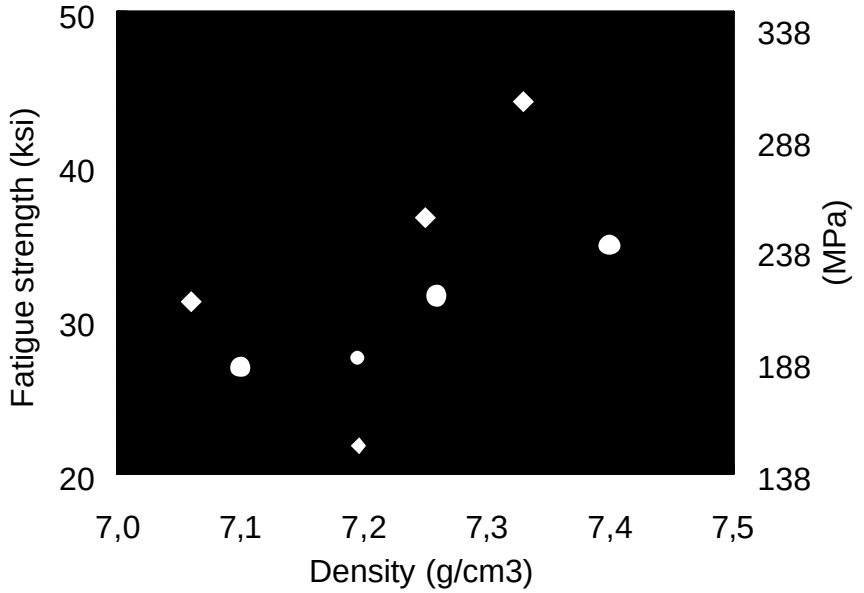


Figure 3. Fatigue strength for 50% survival at $2 \cdot 10^6$ cycles as a function of the density.

The fatigue strength of material D.AE increases with increasing density, see Figure 3. D.HP1 also exhibits this behavior and it is also superior to D.AE at all density levels for the normally cooled material. However, by using rapid cooling D.AE improves to a level above D.HP1.

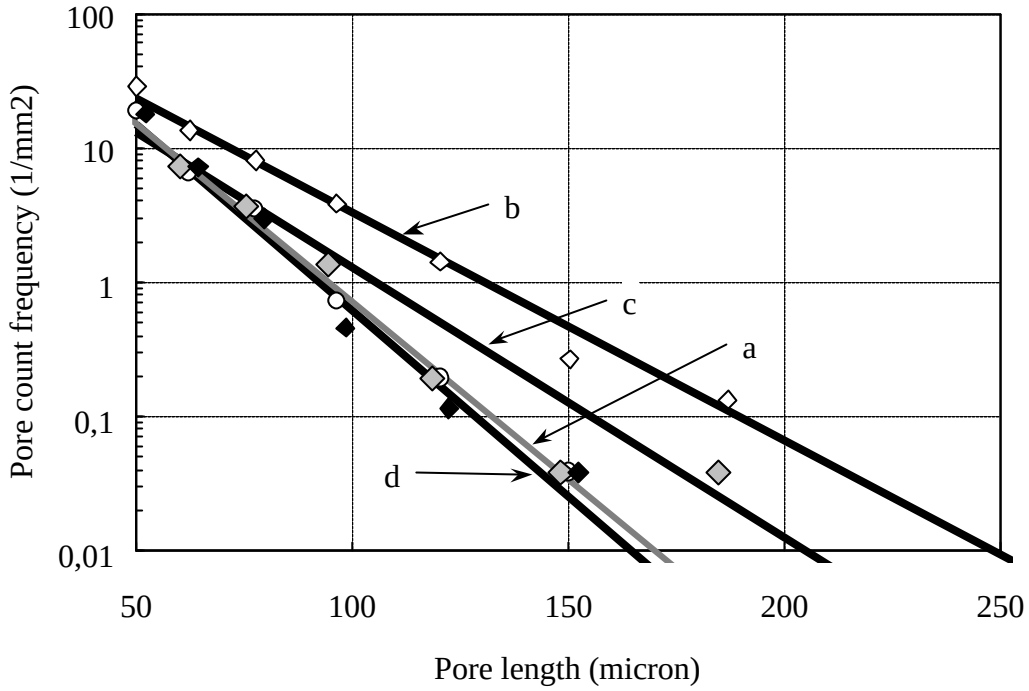


Figure 4. Pore frequency versus pore length. a - D.AE (density 7,28 g/cm^3), b - D.HP1 (density 7,06 g/cm^3), c - D.HP1 (density 7,25 g/cm^3), d - D.HP1 (density 7,35 g/cm^3),

The pore size distributions for materials D.AE and D.HP1 are shown in Figure 4. The pore count frequency is expressed as number of pores (within a given size interval) per area. In the figure it can be seen that all the pore size distributions a re quite similar except the D.HP1 at a density of 7,06 g/cm^3. The pore size distribution for D.HP1 at a density of 7,25 g/cm^3 would have been virtually identical to the D.AE and D.HP1 at a density of 7,35 g/cm^3 if it where not for a single pore of 180 micron length.

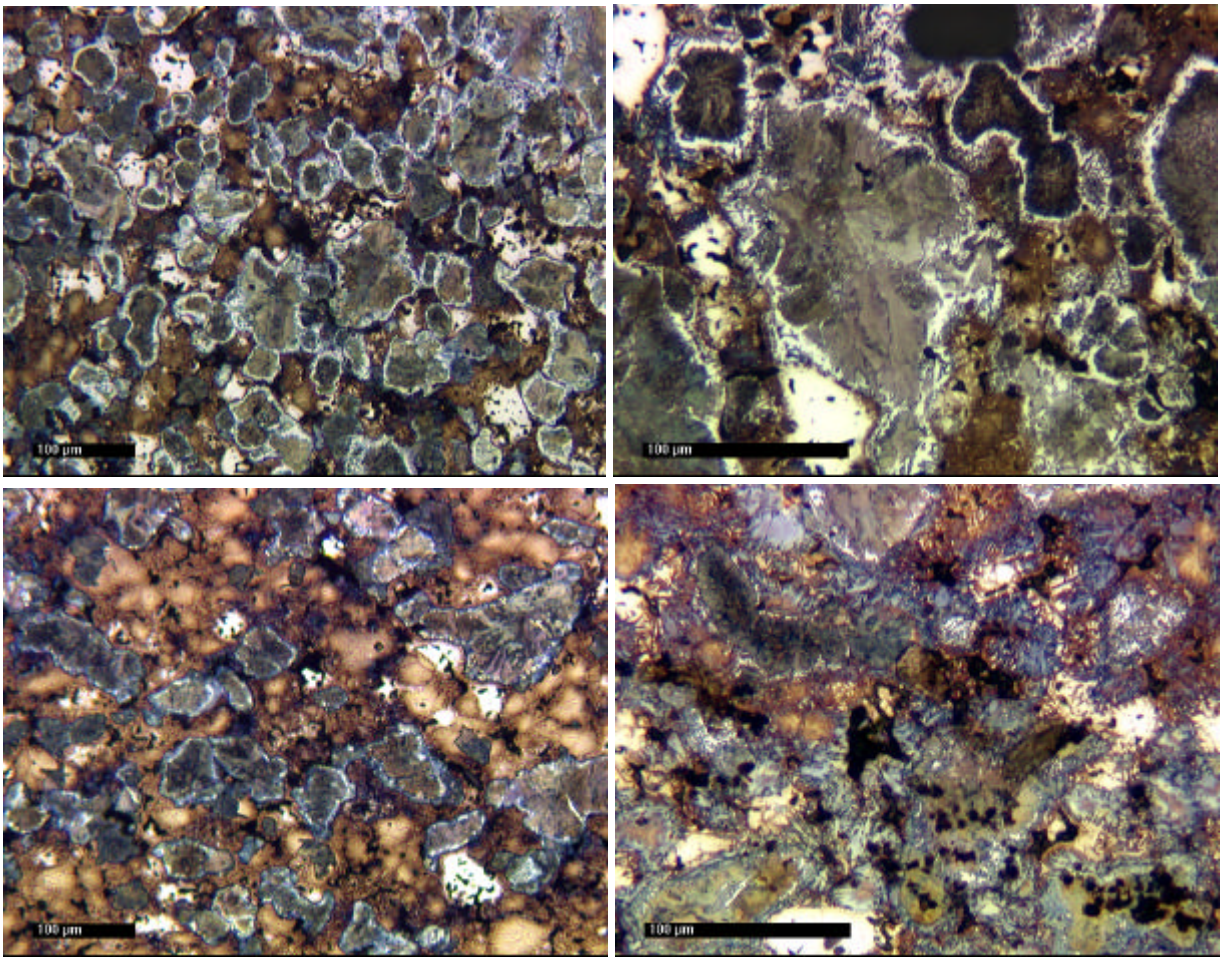


Figure 5. Top row: D.AE normal cooling. Bottom row: D.AE rapid cooling.

Figure 5 shows the microstructure of material D.AE in the normally cooled and rapidly cooled variants. The slower cooling rate results in a microstructure that consists of pearlite islands (former iron particles) in a matrix of martensite, austenite and bainite. The rapidly cooled material exhibits a microstructure that has the same constituents. However, the amount of pearlite is lower and the martensite is dominating the area between the pearlite islands.

The microstructure of material D.HP1 is shown in Figure 6. The major difference in terms of microstructural components and features between the two materials is that what was pearlite islands in the D.AE is bainite in D.HP1.

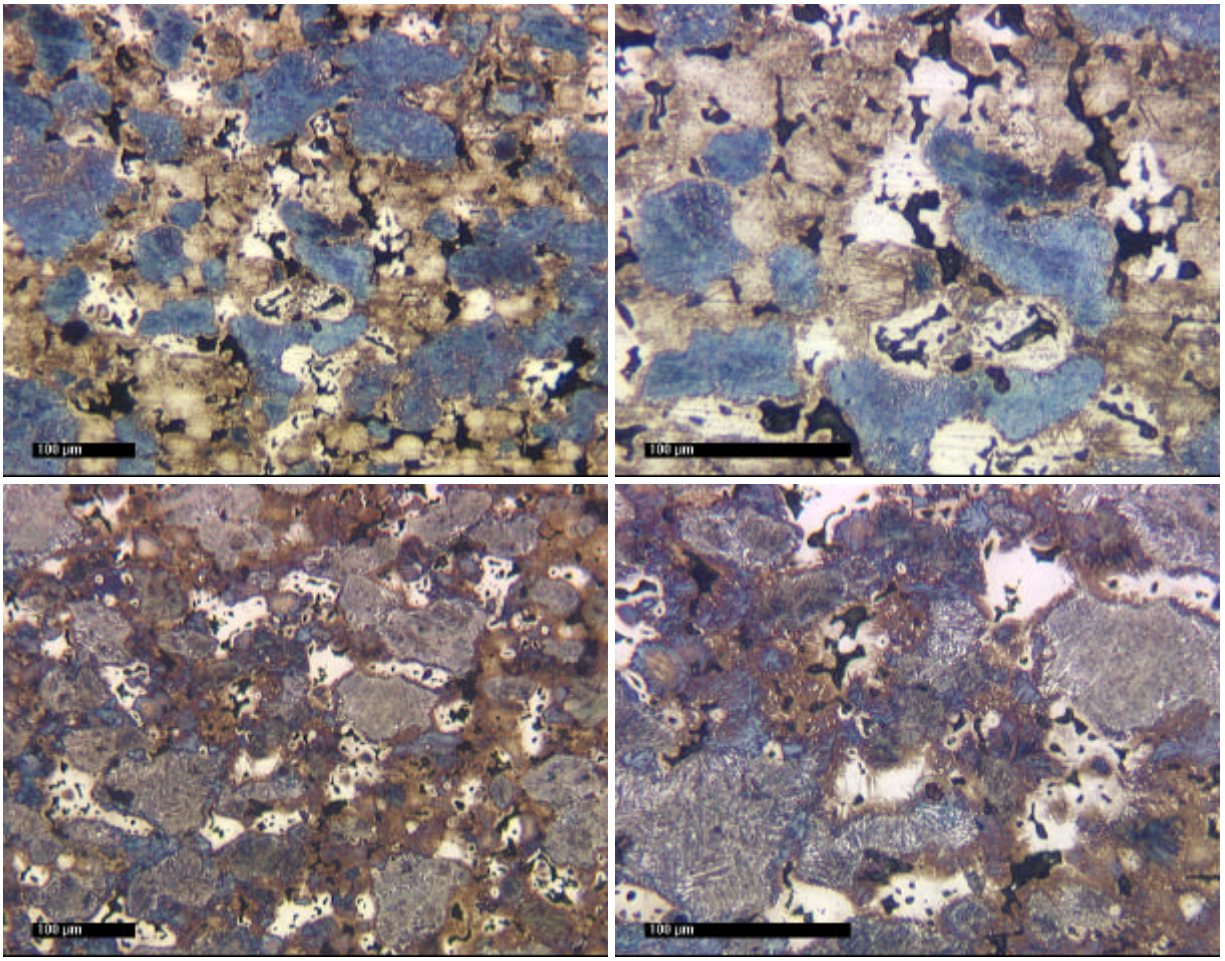


Figure 6. Top row: D.HP1 (density 7,06 g/cm^3). Bottom row: D.HP1 (density 7,35 g/cm^3).

The fracture surfaces of five specimens of material D.HP1 were investigated using scanning electron microscopy with respect to the location of the fracture initiation and the size of the defect (pore), see Table 4. It was found that in most cases (80%) the initiation site is located near (within 100 micron) a corner. The sizes of the defects (pores) for D.HP1 at a density of 7,25 g/cm^3 is 8000 micron^2 for the corner defect and 15000-17000 for the mid side defects This corresponds to a pore length of 90 and 125 micron for the two positions respectively. The length is calculated as the root of the area. This means that in reality the length is higher than this value due to the irregular shape. The fracture initiation sites for the D.HP1 at a density of 7,35 g/cm^3 were found near the corners. The sizes of these defects were 3000-400 micron^2, corresponding to a defect length of 50-60 micron.

Table 4.
Area and location of fracture initiating defects found in a selection of specimens.
Fatigue testing conditions are given for comparison.

Specimen	Position	Area (micron^2)	Length (micron)	Test stress (MPa / ksi)
D.HP1 7,25	corner	8200	91	
D.HP1 7,25	mid-side	15640	125	280 / 41
D.HP1 7,25	mid-side	16480	128	250 / 36
D.HP1 7,35	corner	4000	63	310 / 45
D.HP1 7,35	corner	2730	52	290 / 42

DISCUSSION

The influence of different parameters on the fatigue strength can be divided in the following way [3], for an exhaustive discussion see e.g. [4]: The matrix structure is composed of the microstructural components and the homogeneity of these components. The microstructural components can be ferrite, pearlite, bainite, martensite and austenite. The degree of homogeneity can be described in terms as homogeneous (e.g. a simple pre-alloyed material), heterogeneous (e.g. pre-mixed or diffusion alloyed material). The chemical composition, heat treatment and surface treatment all have a significant influence on these factors. Furthermore, it is well known that the residual stresses can have a significant influence on the fatigue life. These stresses depend on the microstructure of the matrix, the heat treatment, but also on the shape and size of the component. The concept of pore structure is composed of the total porosity (total load bearing cross section), the shape of the porosity (type of stress concentration), the size distribution and the spatial distribution of the pores (influence on crack initiation and propagation).

From Figure 4 it can be seen that the pore size distribution is almost the same for D.AE and D.HP1 at a density near 7,25 g/cm^3, yet there is a significant difference in mechanical properties between the two materials. The D.HP1 has higher fatigue strength, ultimate tensile strength and yield strength, only the elongation to fracture is somewhat lower than D.AE. The introduction of a higher cooling rate on the D.AE has a significant effect on the fatigue strength, yield strength and especially the deformation-hardening rate. The fatigue strength reached is well above the level of D.HP1 at a corresponding density level. The improvement, albeit positive, is not without question marks. The ultimate tensile strength and yield strength of D.AE is still below that of the D.HP1. This means that there must be an additional advantage with the rapid cooling that can not be described in terms of ultimate tensile strength, yield strength, porosity level, pore size distribution, pore shape or pore spatial distribution. It has been shown that a significant step in the development of a fatigue crack is the sub-critical crack growth [5]. The sub-critical crack growth is believed to take place mainly in the soft pearlite islands of former large particle [1]. When these preferred crack initiation sites are transformed into bainite it can be speculated that the sub-critical crack growth is significantly delayed or that the stress necessary to drive the sub-critical crack growth increase.

The effect of density on the fatigue strength is obvious and well known. Material D.AE exhibits an almost linear increase with density in the interval studied. However, as the density increases the nature of the porosity changes. At low densities, below 7,0 g/cm^3, it is the strength of the sintering

necks that control the fatigue strength [4]. At high densities, (above 7,5 g/cm^3?), it is the microstructure of the matrix that dominates the fatigue characteristics of the material. In the density range of high performance P/M components, 7,2 - 7,4 g/cm^3, a combination of good strength at the sintering necks and in the bulk material is desirable. Material D.AE is based on a pure iron powder with all of its alloying elements concentrated on the iron particle surfaces. This means that the sintering necks have a very high proportion of the alloying elements, which in turn means that they will be quite strong. It also means that the iron particles, being devoid of alloying elements, will have a poor hardenability resulting in a soft microstructure for normal cooling rates. However, in the rapidly cooled material this drawback is diminished since cooling rate is sufficient to create a fine pearlite in the iron particles and a larger proportion of martensite.

The D.HP1 with its pre-alloyed base powder has a better hardenability at normal cooling rates compared to the D.AE. The alloying elements at the base powder particle boundaries are almost at the same level as D.AE. This means that the fatigue strength is higher for this material and that the difference is increasing with increasing density.

The pore count frequency is measured on a metallographic sample, i.e. on a surface. In order to translate the frequency valid for a two-dimensional section into a three-dimensional volume it is supposed that the section measurement is valid for a "height" of 25 micron. By multiplying the measured area with the "height" a measured volume can be calculated and as a consequence the pore count intensity per volume. Table 5 and Figure 7 shows the pore size corresponding to exactly one pore of that size in a volume corresponding to the loaded volume of a fatigue test bar (5x5x4 mm^3). The cross section of the fatigue bar is 5x5 mm2 and since two sides of the bar is curved the highly loaded region is considered to be within +/- 2 mm of the minimum cross section. For comparison the volumes corresponding to the edge (4x5x0,1 mm^3) and the corners (4x0,1x0,1 mm^3) are also included. The edge volume consists of the outer 0,1 mm and the corner volume consists of the material within 0,1 mm from the corners.

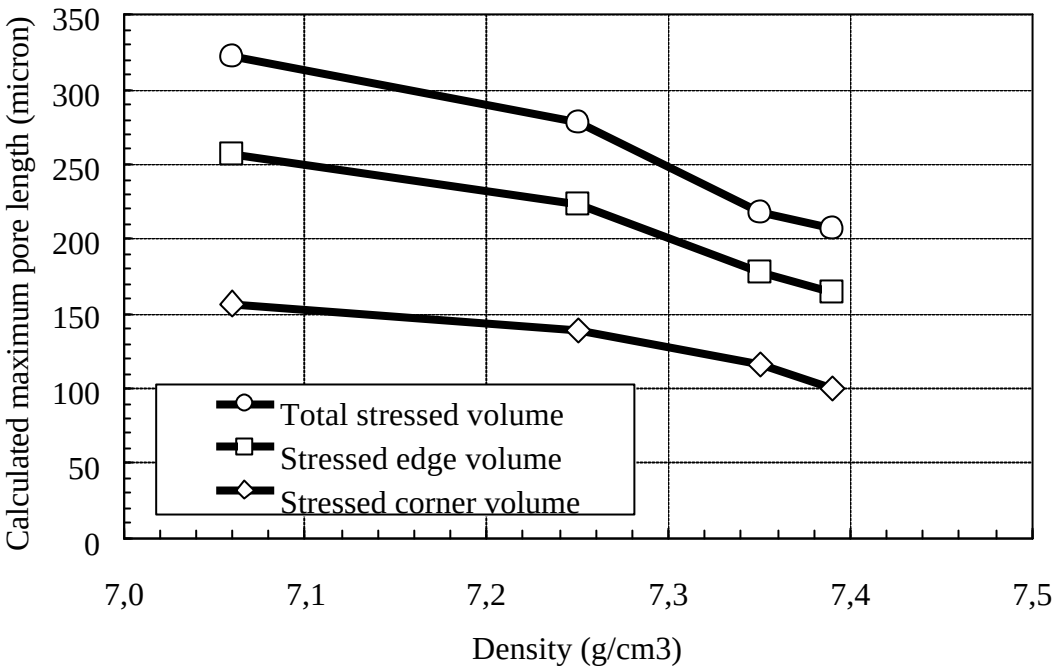


Figure 7. Maximum pore length versus density.

Table 5.

Size of largest pore found in the volume (micron).

Code	In total stressed volume	In stressed edge volume	In stressed corner volume	Density (g/cm^3)	Fatigue strength (MPa / ksi)
D.AE 7,26	225	184	121	7,26	217 / 31
D.HP1 /,06	322	257	157	7,06	215 / 31
D.HP1 7,25	278	223	139	7,25	253 / 37
D.HP1 /,35	218	178	117	7,35	305 / 44

Figure 8 shows the fatigue strength as a function of the maximum pore length as calculated using the total stressed volume as described above. From the figure it can be seen that for a given maximum pore length, the D.HP1 exhibits higher fatigue strength.

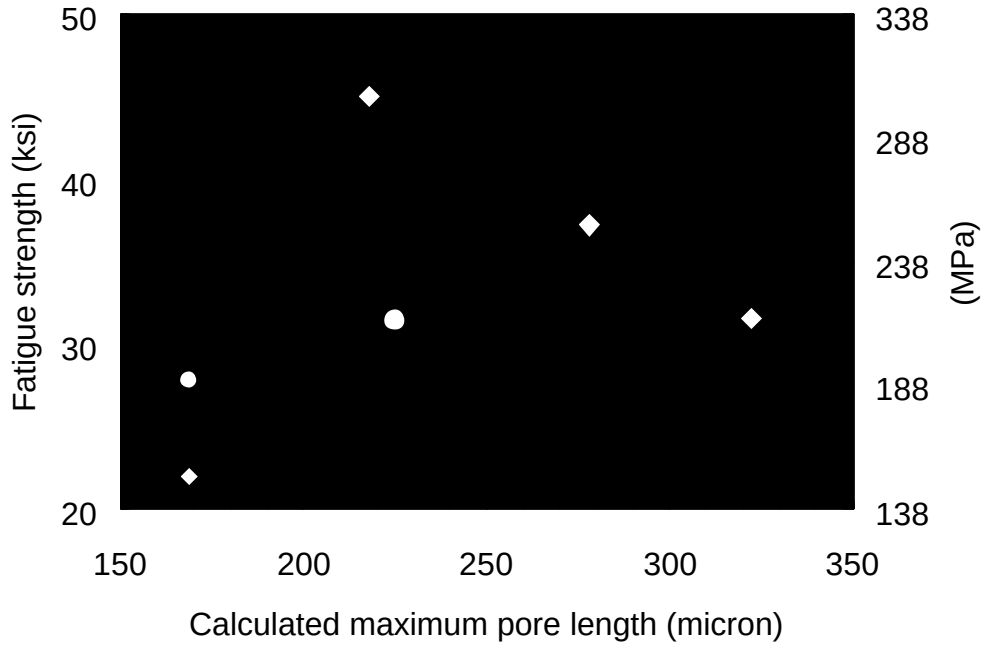


Figure 8. Fatigue strength versus maximum pore length.

The pore size distribution very similar for the highest densities investigated. Measuring the pore size distribution is very time consuming since it is necessary to scan a large area (several cross sections) in order to find a significant number of large pores. This means that the area scanned in the present investigation may not be sufficient to reach the "true" distribution concerning the right hand side of the distribution. However, the distribution, usually seen as a log-normal distribution, may have a natural cut off on the right hand side because of the way the pores are formed. The pores are formed as the volume between the particles. These particles have a size distribution and it is well known that the particle size distribution have an influence on the pore size distribution. Other parameters controlling the pore size distribution are the compaction pressure, compaction method and component size. All in all this means that it is not likely that the right hand side of Figure 4 follows a log-normal distribution. Nevertheless, using the measured pore size distributions it is possible to estimate the size of the largest pore that can be found in a volume of material. The error introduced by the deviation from the log-normal distribution will be that the pore size is over estimated. Most of the fracture initiation sites are located near a corner with the second most popular initiation site near the sides of the test bar. The fact that the fracture initiation sites are located in these positions indicates that there are more factors influencing the crack initiation than the pore population alone. It has been found in similar materials [1] that although the fractures initiate at a defect (pore), a certain sub-critical crack growth must occur in order to reach a critical defect size. The pores of the sizes available are either not large enough or does not cause a stress intensity high enough for the defect to develop into a crack.

CONCLUSION

The fatigue strength of D.HP1 exceeds 300 MPa (44 ksi) at a density of 7,35 g/cm^3.

The fatigue strength of D.HP1 is higher than D.AE at all densities with the difference increasing with density for the material produced with normal cooling rates.

The fatigue strength of D.AE increases significantly when rapid cooling is applied after sintering. The elastic portion of the stress - strain curve increases, causing the yield strength to increase.

REFERENCES

1 O. Mårs, S. Bengtsson and A. Bergmark, "Study of the defect size effect on the endurance limit for sintered steels", Proceedings of the International Conference " Deformation and Fracture in Structural PM Materials, DF PM '99", Piéstany, Slovakia, September 19-22, 1999, pp42-58.

2 J.J. Fulmer and R.J. Causton, "Tensile, Impact and fatigue performance of a new water atomised Low-Alloy Powder - Ancorsteel 85 HP", Advances in Powder Metallurgy 1990. Vol. 2, Pittsburg, Pennsylvania, USA, 20-23 May, (1990), pp459-486.

3 T. Honda. "Trend and future for fatigue characteristics of sintered ferrous products". Journal of the Japan Society of Powder and Powder Metallurgy, 44 (5), (1997) pp475-482

4 A. Hadrboletz and B. Weiss, "Fatigue behaviour of iron based sintered material: a review", International Materials Reviews, Vol 42, No 1, (1997), pp1-44.

5 G. Biallas. "Zyklisches Vervormungsverhalten und Mikrostruktur von Sintereisen und ausgewählten Sinterstählen". Dissertation. Fortschr.-Ber. VDI Reihe 5 Nr 495. VDI Verlag Düsseldorf 1997.